Anal Bioanal Chem (2010) 396:15–29
DOI 10.1007/s00216-009-2959-6

REVIEW

Inorganic mass spectrometry as a tool for characterisation at the nanoscale

Beatriz Fernández · Jose Manuel Costa · Rosario Pereiro · Alfredo Sanz-Medel

Received: 26 May 2009 / Revised: 2 July 2009 / Accepted: 7 July 2009 / Published online: 26 July 2009

Abstract Inorganic mass spectrometry techniques may offer great potential for the characterisation at the nanoscale, because they provide unique elemental information of great value for a better understanding of processes occurring at nanometre-length dimensions. Two main groups of techniques are reviewed: those allowing direct solid analysis with spatial resolution capabilities, i.e. lateral (imaging) and/or in-depth profile, and those for the analysis of liquids containing colloids. In this context, the present capabilities of widespread elemental mass spectrometry techniques such as laser ablation coupled with inductively coupled plasma mass spectrometry (ICP-MS), glow discharge mass spectrometry and secondary ion/neutral mass spectrometry are described and compared through selected examples from various scientific fields. On the other hand, approaches for the characterisation (i.e. size, composition, presence of impurities, etc.) of colloidal solutions containing nanoparticles by the well-established ICP-MS technique are described. In this latter case, the capabilities derived from the on-line coupling of separation techniques such as field-flow fractionation and liquid chromatography with ICP-MS are also assessed. Finally, appealing trends using ICP-MS for bioassays with biomolecules labelled with nanoparticles are delineated.

Keywords Inorganic mass spectrometry · Nanoparticles · Imaging · Spatial resolution · Depth profile analysis

B. Fernández · J. M. Costa · R. Pereiro · A. Sanz-Medel (✉)
Department of Physical and Analytical Chemistry,
Faculty of Chemistry, University of Oviedo,
Julian Clavería 8,
33006 Oviedo, Spain
e-mail: asm@uniovi.es

Introduction

Research at the nanometre scale, aiming at creating novel materials and devices that can operate with performance better than that of conventional systems, is currently of great relevance in many branches of modern science and engineering. Such research involves monitoring, construction and control of systems based on engineered nanodevices and nanostructures. A proper chemical characterisation of nanosystems is crucial today. Moreover, to achieve a deeper understanding of the complex biological processes, adequate analytical tools with spatial resolution in the nanometre region are increasingly needed. Analytical techniques based on mass spectrometry (MS) provide both elemental and molecular information. Their exceptional analytical features [1–3] could be of great advantage for the analytical characterisation at the nanoscale.

MS-based imaging and in-depth profile elemental analyses are not just of interest in materials science and engineering. The direct characterisation of solids at the nanoscale is also extremely important in life sciences, environmental chemistry and Earth science. Here, MS techniques for elemental analysis and characterisation at the nanoscale will be reviewed (Table 1). Two main groups will be dealt with. First, MS techniques for direct solid analysis, including laser ablation (LA) coupled with inductively coupled plasma (ICP) MS, glow discharge (GD) MS and secondary ion MS (SIMS)/secondary neutral MS (SNMS), are reviewed. Then, less investigated approaches for the characterisation of nanoparticles (NPs) as colloidal suspensions using liquid sampling ICP-MS are described and new strategies and applications of ICP-MS in this field are delineated.

Table 1 Comparison of analytical performances and limitations of the most representative approaches of inorganic mass spectrometry (*MS*) techniques for the characterisation at the nanoscale

	Remarkable achievements	Main limitations
Solid-state MS		
LA-ICP-MS	Submicrometre depth resolution (< 300 nm). Elemental imaging in various matrices	Elemental fractionation effects. Lateral resolution in the low-micrometre range
Near-field LA-ICP-MS	Improved lateral and depth resolution and enhanced signal intensity compared with LA-ICP-MS	Instrumental requirements
GD-MS	Depth resolution in the nanometre or even atomic-layer range. Fast sputtering rate (on the order of micrometres per minute)	Limited lateral resolution (on the order of 1–8 mm)
LA-GD-MS	Lateral resolutions of about 20 μm. Signal enhancement compared with GD-MS	Complex calibration method. Instrumental requirements
SIMS	High sensitivity with excellent lateral and depth resolution (in the nanometre range). Imaging with subcellular resolution	Quantification process (large matrix effects). Acquisition time (hours). High vacuum requirements
NanoSIMS	Exceptional lateral resolution (≤150 nm and ≤50 nm \with primary O^{2+} and Cs^{+} ions, respectively)	Instrumental technology (expensive). Acquisition time (hours). High vacuum requirements
SNMS	Matrix effects significantly lower than in SIMS. Low fragmentation of large molecules (using femtosecond laser systems)	Acquisition time (hours). High vacuum requirements
ICP-MS for nanoparticle analysis		
Direct ICP-MS	High elemental sensitivity. Simple method calibration. High potential for bioassays using nanoparticle labels	Restricted to analysis of colloidal nanoparticles or digested samples. Lack of spatial resolution
Coupling of separation techniques and ICP-MS	Allow nanoparticle size distribution analysis. Useful for bioanalytical applications employing nanoparticle labels	Complex and time-consuming. Limited to analysis of nanoparticles in solution

LA laser ablation, *ICP* inductively coupled plasma, *GD* glow discharge, *SIMS* secondary ion mass spectrometry, *SNMS* secondary neutral mass spectrometry

Solid state mass spectrometry techniques

The direct analysis of solid materials avoids the dissolution/digestion of the sample, one of the most time-consuming steps of the analysis, which, on the other hand, increases the risks of sample contamination, analyte loss and loss of spatial information. Over the past few years we have witnessed the continuous growth of techniques which combine the process of surface sampling by a focused laser beam, or by a primary ion beam, with a MS instrument [4–6]. Mass analysers provide multi-elemental capabilities with simple elemental spectra, isotopic information and low limits of detection for many elements.

Typical MS-based direct solid analysis techniques, common today, including GD-MS, LA-ICP-MS and SIMS/SNMS, should be considered to be complementary rather than competitive techniques. SIMS directly produces images with a lateral resolution in the low-micrometre range [7], but owing to the presence of huge matrix effects and the high formation rate of polyatomic ions, SIMS quantification is difficult, as compared with quantification by GD-MS and LA-ICP-MS. On the other hand, LA-ICP-MS experiments have shown that the spatial resolution of LA analysis might be brought down to the nanoscale [8–10], whereas SNMS is not sensitive enough for trace element determinations [11]. A critical comparison of analytical capabilities, with selected examples and trends of LA-ICP-MS, GD-MS and SIMS/SNMS, is presented here as they can be considered the most widespread and powerful inorganic MS techniques currently applied for the direct characterisation of solids at the nanoscale. For other ion sources enabling general solid-state inorganic analysis, the reader is invited to consult more general references [12–15].

Laser ablation inductively coupled plasma mass spectrometry

The combination of LA and ICP-MS has been widely investigated for the direct analysis of solids since 1985 [16]. In addition to the intrinsic detection advantages of ICP-MS [17], the focused laser beam permits the spatial characterisation of heterogeneities in solid materials with a lateral and depth resolution in the low-micrometre and even nanometre range [18].

In the LA process, a short-pulsed high-power laser beam is focused into the solid sample surface in an inert gas atmosphere (e.g. Ar) under atmospheric pressure [19]. The laser beam converts instantaneously a finite volume of the solid sample into a vapour phase aerosol, which is transferred by an Ar or He gas stream into the plasma ion source (i.e. the ICP). The laser-generated aerosol is atomised and ionised there [20]. Finally, the ions formed can be separated and detected using different types of mass analysers, e.g. quadrupole, time of flight (TOF), sector field or multicollector.

One of the main limitations of LA-ICP-MS, basically common to any laser-based sampling technique, is the occurrence of non-stoichiometric effects in the transient signals, defined as elemental fractionation [21]. Fractionation is a complex process, since it can take place during aerosol formation, during transport of the aerosol into the ICP or during aerosol decomposition, atomisation and ionisation in the ICP. A substantial effort has been made in the recent past to understand and reduce, to tolerable levels, such fractionation effects [22–25]. Moreover, matrix effects, non-linear calibrations and the lack of certified reference materials for many types of samples are added inconveniences of LA-ICP-MS for elemental quantification. Experimental parameters, important in LA, such as the wavelength, fluence, pulse width of the laser, the ablation cell design and the carrier gas play an important role in the properties of the laser-generated aerosol. Therefore, the influence of such parameters has been investigated in an attempt to minimise LA-ICP-MS limitations. Interesting developments have been mainly driven so far in two directions: the use of shorter wavelengths and of shorter laser pulses [15, 26]. Both are aimed at a better localisation of the ablation event and, consequently, a more efficient and defined use of the delivered laser pulse energy. In this context, the current availability of robust and compact ultrashort (less than 1 ps) laser systems opens new perspectives in LA analysis owing to the strong confinement of the delivered laser energy [27]. For instance, with use of a femtosecond laser the entire laser energy, on the femtosecond time scale, can be specifically deposited into a well-defined sample surface region and, therefore, the affected material is fully removed with no or minimal damage to the surrounding area. This allows one to obtain chemical information with high spatial resolution and sensitivity.

Depth profile analysis is one of the applications of LA that strongly depends on precise localisation of the applied energy. The principal disadvantage of using longer laser pulses (e.g. nanosecond) is the predominant thermal character of the process, which promotes modification and mixture of different layers of the sample. In contrast to nanosecond LA (ns-LA), fermtosecond LA (fs-LA) pulses generate a plasma with shorter lifetime, allowing more efficient energy transfer to the sample without the interaction of ejected material with the incoming laser pulse [15]. Margetic et al. [28, 29] showed the qualitative depth profiles obtained by fs-LA-TOFMS for semiconductor and metallic samples with coatings in the nanometre range: TiN–TiAlN multilayers of 280-nm thickness on an Fe substrate, and Cr-Ni multilayers of 55-nm thickness on a Si wafer. Despite the Gaussian laser beam profile employed in such experiments, the first layers of such samples could be well resolved in both cases. In addition, Pisonero et al. [30] evaluated the capabilities of fs-LA-ICP–quadrupole MS (QMS) for depth profile analysis of metallic coatings (500-nm Cr layer on a Ni substrate) using a special low-volume ablation cell. The use of low laser fluences (approximately 0.4 J cm^{-2}) together with a low laser repetition rate (1 Hz) provided very low LA rates (less than 6 nm per pulse), which corresponded to only approximately 60 atomic layers per shot. As can be seen in Fig. 1, the crater profiles showed a rather concave shape, probably related to the usage of a non-uniform laser beam. The depth resolution achieved was below 300 nm. A recent application was presented by Mateo et al. [31] for polymer coatings over galvanised steel substrates using fs-LA-ICP-QMS. The combination of fs-LA with a low laser fluence (1.6 J cm^{-2}), low repetition rate (0.2 Hz) and flat-top beam profile provided qualitative profiles with a depth resolution of 240 nm.

At present, the typical lateral resolution of LA-ICP-MS achieved with most commercially available LA systems is in the low-micrometre range (from 5 to 300 μm) [13]. Analysis of biological tissues or cell compartments down to single cells, which require a lateral resolution on the nanometre scale, would be possible by application of near-field (NF) sampling techniques in LA-ICP-MS [32–

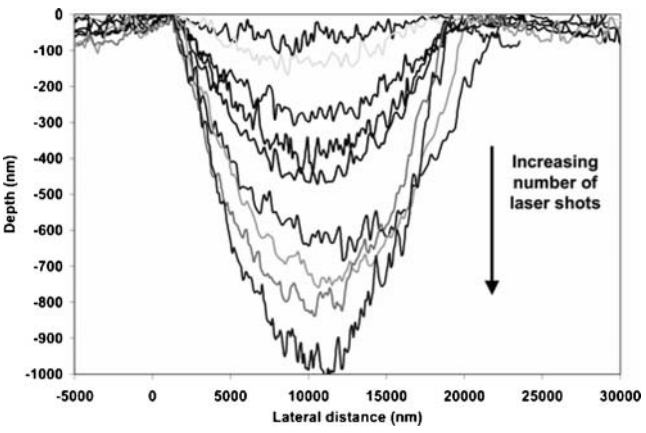

Fig. 1 Crater profiles across the central part of the crater at increasing number of femtosecond laser shots (15, 30, 45, 75, 90, 105, 130 and 150). (From [30]; reproduced with permission of the American Chemical Society)

34]. The idea behind NF-LA consists in the formation of radiation intensity singularities by means of very small conductive objects (e.g. the tip of a thin Ag needle) immersed in the radiation field. Becker et al. [35, 36] have investigated the use of NF-LA-ICP-sector field MS (SFMS) for elemental analysis at the nanometre scale in two-dimensional gels, biological samples and thin Au films. The proposed NF-LA-ICP-SFMS arrangement employed thin Ag needles (d~180–250 nm) electrolytically etched, and the distance between the needle and the sample surface was controlled by measuring the tunnel current. When the needle was at a defined distance from the sample surface (approximately 200 nm), laser shots of a defocused laser beam caused a local enhancement of the incident laser energy on the needle tip which was sufficient to ablate the sample. Spatial resolution in the 100-nm range was obtained. ^{197}Au and ^{28}Si signals showed an about 100-fold increase of the ion intensity when the needle was at a distance of about 200 nm from the surface, in contrast to the case where it was far away from the sample.

Melt inclusions have become an increasingly powerful source of information about different processes in Earth science. LA-ICP-MS dating provides geochemists with invaluable information on small-scale heterogeneities in rocks and geological environments [37, 38]. Horvath et al. [39] have investigated Xe gas inclusions in nuclear fuel by using LA-ICP-QMS and LA-ICP–multicollector MS. In nuclear fuel, approximately 20% of the fission products are gaseous and these gas atoms in the fuel matrix can occur in nanometre-sized intragranular bubbles and in micrometre-sized intergranular pores. Although further improvements in spatial resolution are required to analyse single gas inclusions, with use of small laser spot sizes (in the range 4–200 µm, depending on the LA system) calibration methods were successfully applied to determine Xe in small gaseous inclusions.

Finally, the application of LA-ICP-MS as a sensitive imaging technique to determine quantitative distributions of metals, non-metals and organic compounds in thin sections of biological and environmental samples should be highlighted [40–42]. Quantitative imaging of elements by MS in biological tissues is a challenging task in analytical chemistry and is relevant in different areas of biological and medical research. Becker et al. [3, 9, 43] have investigated two-dimensional imaging of trace elements (e.g. Cu, Zn, Pb, P and S) in thin tissue sections of human and rat brains by LA-ICP-SFMS to employ them as indicators to monitor health risks. For instance, a spatially inhomogeneous elemental distribution could be easily found through a human brain hemisphere. Whereas Cu and Zn distributions showed a clear laminar pattern and higher concentrations (in the microgram per gram range) in the hippocampus region, Pb showed more homogeneity and a lower concentration (in the nanogram per gram range). Concerning the metal distribution in small cerebral tumours induced into rat brains, Cu showed a heterogeneous distribution within the tumour, corresponding to areas of different degrees of vitality and necrosis, as well as a higher concentration than in the healthy control brain (see Fig. 2). Furthermore, there is currently increasing interest in using plants for phytoremediation of contaminated areas with metals and LA-ICP-MS has been investigated for quantitative imaging of nutrient and toxic elements in plant tissues [42, 44, 45]. To explore the effect of Cu stress on nutrient uptake and accumulation in Cu-tolerant plant leaves, K, Mg, Mn, P, S and B were studied by quantitative imaging

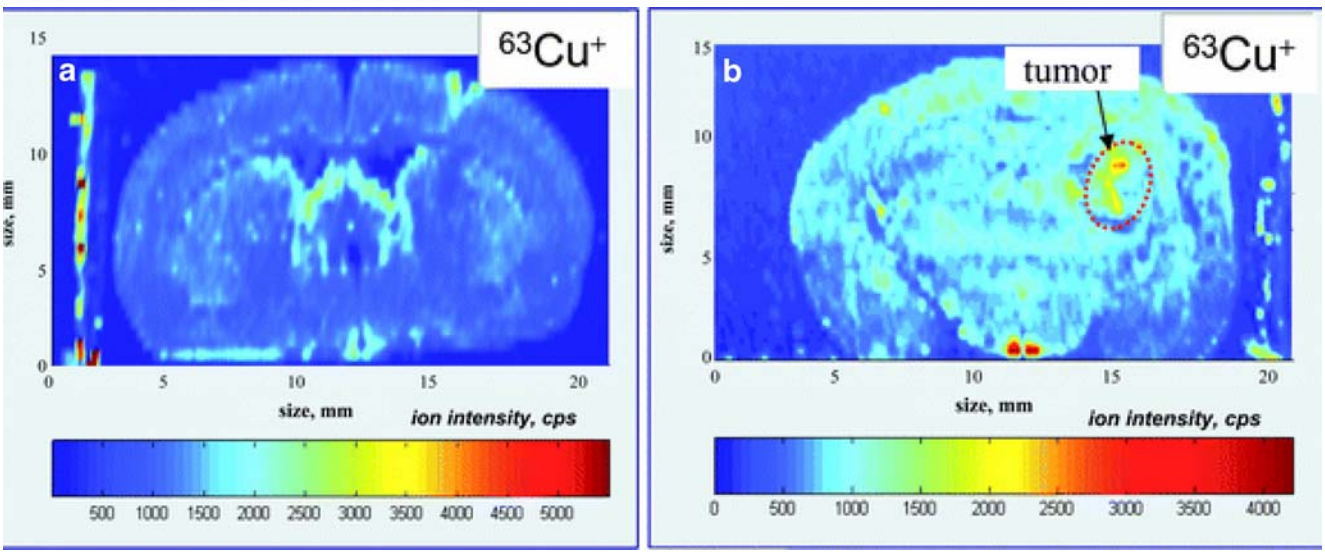

Fig. 2 Cu distribution in two cross-sections of rat brain with a tumour region (**b**) compared with control tissue (**a**). (From [9]; reproduced with permission of the Royal Society of Chemistry)

LA-ICP-SFMS [44, 45]. Two-dimensional images showed that in the newly formed leaves the concentrations of the measured essential elements (K, Mg, Mn, P, S and B) were lower than those in the older leaves. Moreover, Cu stress induced K, Mg, Mn, P and S accumulation in the newly formed leaves of the plant, whereas B was not significantly affected [45].

Glow discharge mass spectrometry

The combination of GDs with MS is accepted as a powerful technique for the direct determination of trace impurities and depth profile analysis in solid samples [5]. The analysis of the sputtered material as a function of the sputtering time allows the determination of the compositional distribution of a thin film versus the distance from the original surface [46]. The atomisation and ionisation processes in GD are separated in space and time, resulting in little matrix dependence, so quantification can be possible without the absolute need for matrix-matched standards. Moreover, the coupling of GDs and MS detection offers several important capabilities, such as high depth resolution (approximately nanometre), fast sputtering rate (on the order of micrometres per minute), multielemental analysis, isotopic information, low limits of detection (in the range of micrograms per gram to nanograms per gram) and ease of use [5, 14].

The most common operation mode in GD spectrometry is the application of a direct current voltage, as it has been demonstrated to be an easy-to-handle technique for electrically conductive samples. Radiofrequency (rf) GD can also be applied to electrically non-conductive samples, broadening GD applications to glass and ceramic films, implants, bones, semiconductors, environmental samples, etc. [47]. Additionally, one of the most interesting developments in GDs in recent years has been the introduction of pulsed GDs [48, 49]. A pulsed GD is created by periodically applying a signal of high power with millisecond or microsecond duration. Pulsed GDs offer a real possibility for separating elemental and molecular information owing to the temporal distribution of power (with time domains called prepeak, plateau and afterglow) [50]. Furthermore, the pulsed mode gives high instantaneous power, increasing the atomisation, excitation and ionisation processes without inducing thermal degradation of the sample [51].

GD-SFMS provides low limits of detection (approximately micrograms per gram) and high mass resolution (up to 10,000). Nevertheless, all GD-SFMS systems are sequential in nature, which is a serious limitation for the analysis of fast signals (e.g. depth profile analysis). At present, GD-SFMS instruments are the only GD-MS instruments commercially available and are manufactured by Thermo Fischer Scientific. Alternatively, TOF mass analysers offer interesting features, such as quasi-simultaneous detection of a large mass range (from H to macromolecules), higher mass resolving power compared with QMS, lower cost compared with high-resolution SFMS and a high spectral acquisition rate, which allows the measurement of transient ion signals [52, 53], thus offering a great potential for thin and ultrathin solid films [54]. GD-TOFMS systems are not yet commercially available, although new prototypes are currently under development in a European project (EU through FP6 contract STREP-NMP).

Rf-GDs have demonstrated depth resolution in the nanometre or even atomic-layer range [5, 55], both with optical emission spectrometry (OES) and MS. For example, Hoffmann et al. [56] compared GDs with SNMS for the evaluation of a multilayer system (5-nm layers of Ni and Cr) on a Si substrate. They showed that, although similar depth resolutions can be obtained by both techniques, the analysis time was much shorter with GD. Similarly, the capabilities of two rf-GD devices (a commercial GD-OES instrument from Jobin Yvon and a home-made GD coupled to a TOFMS instrument from LECO) were assessed by Pisonero et al. [46] for the analysis of thin films on thick glasses (27-nm Si_3N_4/15-nm Nb/6-nm Si_3N_4 on a 6-mm glass substrate). Moreover, it should be highlighted that the first example of depth profile analysis of a layer of subnanometre thickness using GDs was presented by Shimizu et al. [57] for the analysis of a monolayer of thiourea adsorbed on a Cu substrate (in this case the experiments were carried out by OES).

Pulsed rf-GDs are particularly advantageous for the analysis of heat-sensitive materials, such as glasses and polymers [58, 59]. Studies on pulsed rf-GDs coupled with MS are still scarce, although the combination with TOFMS is particularly promising. Muñiz et al. [60] investigated the analytical capabilities of a pulsed rf-GD-TOFMS system for the analysis of multinanolayers deposited on glass. The system allows the acquisition of complete mass spectra at different pulse time domains within the same run and, under the optimised GD operating conditions, the sputtering time required to remove the coating (about 200-nm thickness) was only 160 s. The high depth resolution obtained was able to resolve the layers of the coating, making it possible to distinguish two internal layers of 10-nm thickness. Hohl et al. [61] showed the qualitative depth profile obtained by pulsed rf-GD-TOFMS of an ultrathin Cr-delta layer embedded in a thin alumina coating. As can be seen in Fig. 3, the 2-nm Cr marker was well discriminated, demonstrating the excellent depth resolution that can be obtained using pulsed rf-GDs. Additionally, pulsed rf-GD-TOFMS has recently been evaluated for the analysis of polymers [62, 63]. Thin films of different

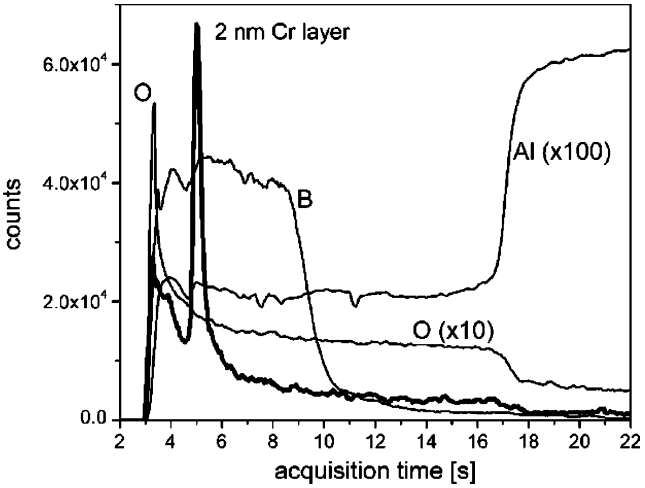

Fig. 3 Depth profile of an Al sample with an aluminium oxide surface of 240-nm thickness and enclosing a 2-nm Cr marker. (From [61]; reproduced with permission of Wiley Interscience)

polymers deposited on Si substrates were successfully analysed, and both elemental and molecular information as well as positive and negative ions could be obtained along the qualitative profiles.

One of the major limitations of GDs is the poor lateral resolution. GDs show restricted lateral resolution on the order of 1-8 mm, which is directly related to the size of the sampling orifice. Taking into account the analytical performances of LA and GD sources, a MS technique combining LA and GD would appear very attractive. The laser can be used to ablate the material from the sample surface, whereas the GD source is used for postionisation of the ablated material. Furthermore, the sampling and ionisation steps are spatially and temporally separated and, thus, can be independently optimised. At present, such a combination is almost unexplored [64–66]. Tarik et al. [66] have recently investigated the analytical capabilities of LA coupled with pulsed GD-TOFMS. Direct ablation during the afterglow of the pulsed GD led to an ion signal enhancement of up to a factor of 7, compared with the ablation process alone under the same experimental conditions. Additionally, Shelley et al. [67] have studied the combination of LA and a flowing atmospheric pressure afterglow for ambient mass-spectral imaging. Two-dimensional mass-spectral images were generated by scanning the laser beam across the sample surface and spatial resolutions of approximately 20 μm have been achieved.

Secondary ion mass spectrometry and sputtered neutral mass spectrometry

SIMS is based on the use of a focused primary ion beam of sufficiently high energy (between 0.25 and 30 keV) to bombard the sample surface. The primary ions penetrate into the solid surface to different depths (in the range 1–10 nm) and transfer their kinetic energy through binary collisions to the atoms of the target. Then, the target atoms are displaced from their original sites, colliding with other target atoms and, thus, producing a collision cascade until the transferred energy is insufficient to cause atom displacement. Collision cascades that reach the surface may cause the ejection of sample material from the first atomic layers (sputtering process). Most of these sputtered particles are neutral, but some are charged (secondary ions). The secondary ions are then collected, separated in a mass analyser and detected. In the case of SNMS, the sputtered ions are suppressed by a repeller voltage, whereas the sputtered neutrals are postionised and then analysed in the mass spectrometer [68, 69].

In static SIMS, the data acquired are characteristic of the surface. In contrast, in dynamic SIMS, the sample is sputtered and data are obtained as a function of depth. Dynamic SIMS is used for the analysis of atoms or small molecular fragments, whereas static SIMS can be used for the analysis of larger fragments from organic molecules. Moreover, there are two ways of operating a SIMS instrument; the microscope mode and the microprobe mode [14]. In the microscope mode, a defocused primary ion beam (5–300 μm) is used to investigate a large surface. The secondary ions are then transmitted to a mass spectrometer, which generally uses an image detector. In the microprobe mode, a focused primary ion beam (less than 10 μm) is used for investigating a very small portion of the surface and detecting inclusions in bulk material. Here, the lateral resolution is defined by the primary ion beam size (an electron multiplier is usually employed for detection).

The versatility of SIMS is mainly due to the combination of its high sensitivity with good topographic resolution, both in-depth and lateral. The energy of the primary ions is closely related to the spatial resolution achieved and, thus, higher energies result in better focused beams (higher lateral resolution), and also in a higher sputtering rate, which improves the sensitivity but could degrade the depth resolution. Primary ions commonly used are Cs^+, O_2^+, Ar^+, Xe^+ and Ga^+ as well as the more recently reported Bi and Au cluster ions (Au_n^{z+}, Bi_n^{z+}) and even C_{60}^+ [70]. In comparison with the use of noble gas primary ions (Ar^+ and Xe^+), the use of O_2^+ and Cs^+ increases the ionisation probability for species that tend to form cations and anions, respectively. Moreover, Ga^+ is employed to obtain high lateral resolutions owing to the finely delivered focused beam [71], whereas the recent use of C_{60}^+, Bi and Au clusters for the analysis of polymers and biomolecules allows yield improvement of high molecular mass fragments [6].

Concerning the type of mass analyser used, only one specific ion image can be acquired at a time using

sequential mass analysers, so serious limitations can be found in terms of in-depth resolution and correlation of sequential images of various species. To overcome this difficulty, TOF spectrometers have been widely used [72, 73]. Imaging MS has the unique ability to acquire the spatial distribution of a wide range of atoms, isotopes and molecules and, for many years, commercially available TOF-SIMS instruments have been able to produce mass resolution of several thousand in imaging mode [74, 75]. Few surface imaging techniques can rival the combination of detailed chemical information and relatively high spatial resolution provided by TOF-SIMS imaging.

SIMS and SNMS have been successfully used to image and quantify targeted compounds, intrinsic elements and molecules with subcellular resolution in single cells of both cell cultures and tissues [76–79]. In such applications, a finely focused primary ion beam sweeps the sample in a raster pattern and, simultaneously, the secondary ion intensities are saved as a function of the beam position. Barnes et al. [80] have recently investigated the potential of TOF-SIMS to image contamination distributions in microelectronic devices. To optimise interconnect metallisation performance in terms of resistivity, the detection and localisation of low levels of contaminants (e.g. Cl and S) resulting from the electrochemical deposition process used in microelectronics is required. TOF-SIMS spatially resolved images of Cl and Cu were used to study whether the Cl contamination in Cu films is homogeneously distributed or localised at the grain boundaries. Figure 4 shows secondary ion images from a patterned test structure. In Fig. 4b and d, some contrast is visible in the total ion image, suggesting a grain structure in the central line, but no Cl is visible in this line. Moreover, nanoSIMS technology has recently extended isotopic studies to considerably smaller sample scales (below 500 nm) [81]. In this case, the primary beam path is strongly modified to become coaxial with the secondary beam within the objective column, and this configuration imposes the use of primary ions of sign opposite to those of the observed secondary ions. For example, CAMECA NanoSIMS 50 equipment has demonstrated a high lateral resolution (150 nm or less and 50 nm or less with primary O_2^+ and Cs^+ ions, respectively), the ability to detect simultaneously five different ions from the same microvolume and a very good transmission even at high

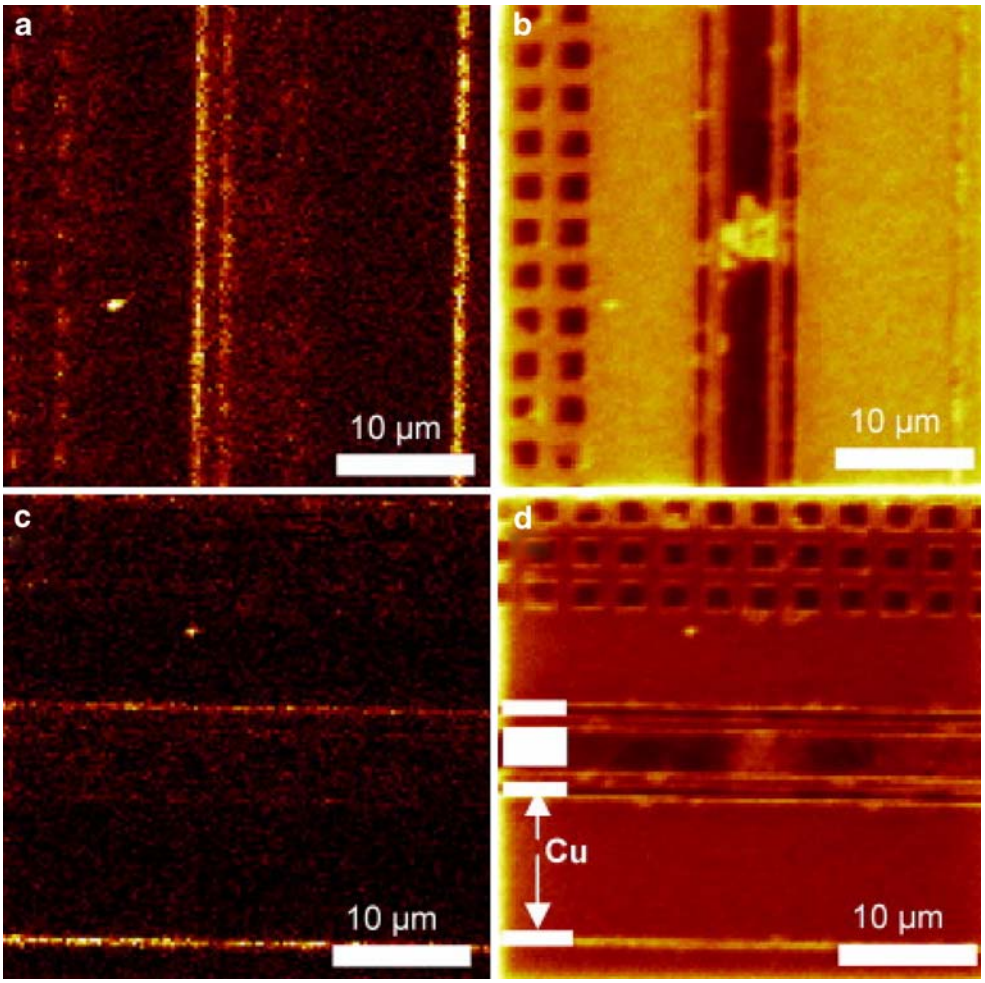

Fig. 4 Time of flight secondary ion mass spectrometry negative secondary images of **a**, **c** $^{35}Cl^-$ and **b**, **d** total ion from Cu lines in a test structure showing a difference in Cl^- intensity between different Cu lines. The images in **c** and **d** are from exactly the same area as the images in **a** and **b** but with the sample rotated by 90º. The Bi analysis gun was used with Cs presputtering to remove surface oxide. The image of the total ion intensity in **d** is darker than the image in **b** because it was the second image taken on the same area and the Cs concentration had decreased because of sputtering with the Bi analysis gun during the first image. (From [80]; reproduced with permission of Elsevier)

mass resolution [82]. During the last few years, nanoSIMS technology has been strongly investigated for a wide range of applications, including isotopic measurements of presolar silicon carbide grains from supernovae [83], for imaging of As traces in human hair [84], to test the toxic effects of Al, Co and Cr particles in cells [82], to study the localisation of Fe in Alzheimer's disease hippocampus [85] and for surface chemical analysis of DNA microarrays [79].

Despite SIMS showing excellent elemental sensitivity, the capability for spatial resolution in three dimensions as well as potential for identification of chemical compounds, deficiencies still exist in the quantification process [13, 69]. It is worth stressing that large matrix effects occur in SIMS, which do not even allow a reliable semiquantitative analysis, whereas in SNMS (where the evaporation and ionisation processes are decoupled) matrix effects are significantly lower. On the other hand, although applications have been reported for imaging of biotissues using SIMS and SNMS, it should be stressed that the difficulties to desorb big proteins as well as the low sensitivity achieved are two important limitations of such MS techniques. The recent development of a new system for imaging MS using megaelectronvolt ion beams (MeV-SIMS) has demonstrated a more than 1,000-fold increase in molecular ion yield from a peptide sample (1,154 Da), compared with kiloelectronvolt ion irradiation [86]. This significant enhancement of the molecular ion yield is attributed to electronic excitation induced in the near-surface region by the impact of high-energy ions, and these results indicate that the MeV-SIMS technique can be a powerful tool for high-resolution imaging in the mass range from 100 Da to over 1,000 Da. Additionally, the use of femtosecond lasers for the ionisation step in laser SNMS has been shown to increase the sensitivity as well as to reduce the fragmentation of large molecules, otherwise a limiting factor for the biomolecule identification capability of the SNMS technique [87]. Laser postionisation SNMS has been successfully evaluated for elemental and molecular imaging at the subcellular level for cell cultures and tissues [88–90], for pharmaceutical studies [91] and for the development of targeted drugs [92].

Finally, it should be highlighted that SIMS and SNMS are currently considered the most widespread inorganic MS techniques for depth profile analysis at the nanoscale of modern materials of technological interest. SIMS and SNMS allow depth profile analysis with a depth resolution in the low-nanometre range of hard coatings [93], atmospheric aerosol particles (with aerodynamic diameters on the order of 25–200 nm) [94], nano-objects (nanowhiskers consist of fibres of about 2-nm diameter) [95] and nanoscale multilayers [96–100]. Figure 5 shows the depth profiles obtained by SNMS for a triple-layer system used for gas sensor microdevices (Fig. 5a) and for an electrodeposited multilayer sample with magnetic properties (Fig. 5b), respectively. As can be seen, SNMS permits investigation of conductive and non-conductive layers at a depth resolution better than 10 nm. Moreover, Escobar et al. [101] have recently compared the capabilities to perform depth profile analysis of nanometre-metal multilayers (thin metal layers with a thickness in the range 5–500 nm) using different ion-probing techniques (Rutherford backscattering spectrometry, SIMS and GD-OES). The analyses demonstrated that SIMS can resolve ultrathin layers (down to 2.5 nm) of Cr buried deep in structures (more than 1 μm).

Inductively coupled plasma mass spectrometry for detection, quantification and characterisation of nanoparticles in solution

In recent years, ICP-MS has become one of the most versatile and sensitive tools for elemental analysis in

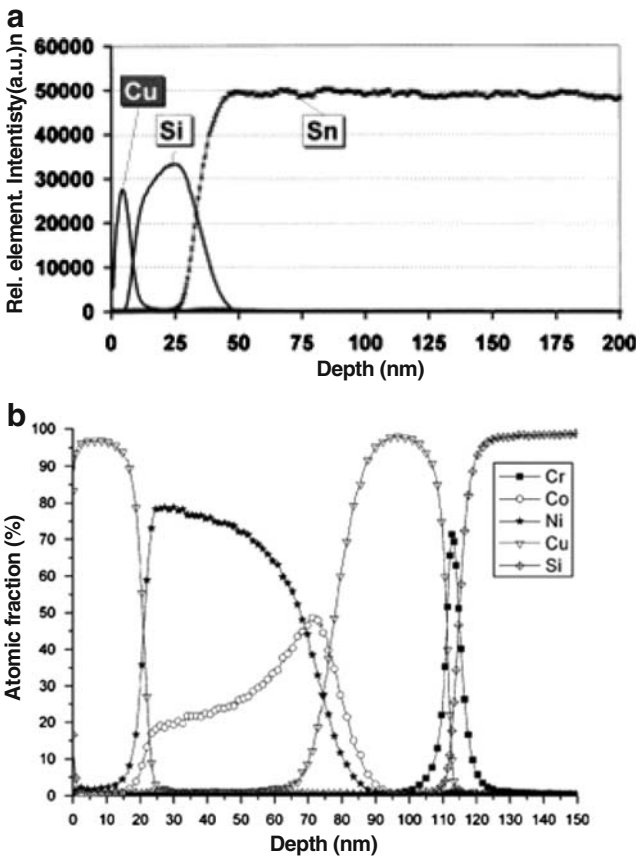

Fig. 5 Examples of depth profiles obtained by secondary neutral mass spectrometry (SNMS). **a** SNMS depth profile of CuO/SiO_2 (not annealed)/SnO_2 (not annealed) after preparation. **b** SNMS depth profile of a sample consisting of Cu (20 nm)/Co–Ni–Cu (50 nm)/Cu (20 nm)/Cu (20 nm)/Cr (5 nm)/Si substrate. (**a** From [96]; reproduced with permission of Elsevier. **b** From [100]; reproduced with permission of Elsevier)

analytical chemistry [17, 102, 103]. Most elements can be ionised in the ICP source. Routinely achievable sub-nanogram per litre detection limits have permitted the detection of ultratrace metal species in complex matrices. In addition, the dynamic range of ICP-MS routinely exceeds 6 orders of magnitude, allowing detection of both major constituents and trace components at the same sample dilution. Moreover, quantification is rather easy and requires only standard solutions of inorganic elements. Furthermore, ICP-MS allows the straightforward use of isotopic-dilution techniques for most accurate measurements.

Applications of ICP-MS to biomolecules have been especially boosted by the present commercial availability of collision and reaction cells and high-resolution (double-focusing) ICP-MS instrumentation, as well as by the development of suitable interfaces for coupling of ICP-MS with separation techniques [104]. Moreover, recently, ICP-MS has been demonstrated to be a highly valuable tool for ultrasensitive detection and characterisation of metalloid-containing NPs. Therefore, applications of ICP-MS as a tool for elemental detection and characterisation of NPs will be discussed next.

Direct inductively coupled plasma mass spectrometry analysis of liquid samples containing metal-based nanoparticles

Both colloidal and ionic solutions may be analysed with ICP-based spectrometry techniques. The ICP can easily vaporise, atomise and ionise NPs with radii of typically 5–100 nm in solution. Thus, ICP-MS is being exploited as a highly sensitive and selective analytical tool for the elemental characterisation of colloidal NPs in different applications.

ICP-MS has already demonstrated its potential as a fast and reliable technique well suited for quantification of NPs in solution. Additionally, ICP-MS determinations of total elemental concentrations of such colloidal suspensions have also been proposed for the characterisation of NPs all along the synthesis process. Moreover, functional groups present in biomolecules can be labelled with appropriate NPs which would then be determined quantitatively via ICP-MS. Applications of ICP-MS to colloidal solutions of NPs have been reported during the last few years and representative examples are described in the next sections.

Elemental characterisation of engineered nanoparticles by inductively coupled plasma mass spectrometry

So far, synthesis control and analytical characterisation of colloidal NPs has been mainly carried out using spectrophotometry, photoluminescence, X-ray photoelectron spectroscopy, X-ray diffraction and electron microscopy techniques, among others [105]. However, only a few papers have paid attention so far to the elemental content of the nanomaterials and its influence on their physicochemical properties. In this context, the inherent quantitative character of the ICP-MS response could be of great value to achieve a precise elemental characterisation of the nanomaterials, which, in turn, could shed new light on their properties and allow optimisation of their synthesis.

Most recently, ICP-MS has been employed in the characterisation of CdTeSe and CdTeS ternary semiconductor nanocrystals or quantum dots (QDs) synthesised using a chemical aerosol flow procedure [106]. Data from ICP-MS showed that the internal structure of the synthesised QDs had a gradient in the Se to Te concentration ratio with a CdTe-rich core.

Degueldre et al. [107] developed a method based on ICP-MS detection for the investigation of the size distribution of Au NPs in colloidal suspensions. ICP-MS was run here in "single-particle operation mode" (based on the nebulisation of very dilute solutions, so that statistically only one NP reaches the plasma within a certain time range, thus causing an intensity signal at the MS detector proportional to the size of that particle). Using a colloid suspension injection system coupled to the ICP-MS system, the authors investigated particles with diameters of 80–250 nm (they determined a detection limit of the method for individually introduced particles of 25 nm). Considering that the Au NPs typically used in bioapplications have smaller diameters, the overall ion transfer efficiency in the mass spectrometer should be improved to detect smaller nanoparticles [107].

ICP-MS analysis of colloidal suspensions of PbSe nanocrystals, combined with spectrophotometry and transmission electron microscopy (TEM), was used to determine the PbSe nanocrystal composition [108]. Samples were prepared by drying a known amount of PbSe NPs under a strong N_2 flow and digesting them in 10 mL of HNO_3. With use of the ICP-MS system, both the Pb and the Se concentrations were determined, from which the Pb to Se ratio was calculated. Combination of the ICP-MS results with detailed modelling of the nanocrystals allowed the NP composition to determined. The ICP-MS results did not show a 1:1 Pb to Se ratio. A systematic excess of lead was observed, scaling with the NP surface area. The observed ratio is consistent with a faceted spherical NP model, composed of a quasi-stoichiometric nanocrystal core terminated by a Pb surface shell.

Most recently, ICP-MS analysis of colloidal suspensions of QDs, with a core of CdSe and a shell of ZnS, was used to study the distribution of elements (Cd, Se, Zn and S) in the core and shell of the nanocrystals [109]. The accurate quantitative ICP-MS measurements (using isotopic-dilution

analysis) of the NP colloidal suspensions were used to investigate the kinetics and to characterise the elemental composition of the core and shell with time. The non-stoichiometric nature of the NP core (Cd excess) was also demonstrated. Moreover, the elemental data obtained provided experimental proof of a mixed-shell CdS/ZnS growing over the CdSe QD core. The influence of the molar ratios of the elemental precursors used on NP size has also been studied, and molecular techniques were employed in combination with ICP-MS to calculate the number of atoms of Se and Cd existing in an individual QD [109].

Calero-DdelC and Rinaldi [110] optimised a novel process for synthesis of Co-substituted ferrite NPs with a narrow size distribution. The NPs synthesised under the different experimental conditions were characterised by techniques such as X-ray diffraction, Fourier transform infrared spectroscopy and ICP-MS, employed to confirm the presence of Co in the synthesised NPs.

As demonstrated in the above-mentioned reports, ICP-MS not only allows a reliable determination of the elemental NP content; from such measurements the number of atoms per synthesised individual NP can also be calculated. These data could be most valuable for an appropriate characterisation of the NPs, also allowing a better control of the NP synthesis process.

Inductively coupled plasma mass spectrometry for quantification of colloidal nanoparticles in biotoxicology studies

Over the past few years, many studies have been conducted to establish the biodistribution patterns of NPs in living species. Such information is of great value to understand the possible toxic impact after a possible exposure of a given organism to the NPs studied. Moreover, today, to optimise NPs in pharmacology, the biodistribution profiles of NPs (e.g. used as drug carriers) should be established.

The high elemental sensitivity typically achievable with ICP-MS and the low elemental concentrations usually present in living species of those elements constituting the NPs (e.g. Au, Ag and Cd) ensure a relatively low spectral background. Very recently, ICP-MS was used to study the biodistribution of Au NPs after intravenous administration in mice [111, 112]. Au NPs of different sizes, mainly 15, 50, 100 and 200 nm, were synthesised. The NPs (suspended in sodium alginate solution) were then administered to mice and, 24 h after administration, blood and various tissues/organs were collected to obtain the biodistribution of the NPs in the mice. The determination of Au in the samples was carried out quantitatively by ICP-MS. The results revealed that the tissue distribution of Au NPs was size-dependent, with the smallest NPs (15 nm) showing the most widespread organ distribution [111]. Moreover, for all Au NP sizes the majority of the Au was demonstrated to be present in liver and spleen [112].

A similar study was performed to evaluate the distribution and interaction of Ag NPs with cells in the brain [113] and to study the biological behaviour of QDs in vivo [114]. Male mice were intravenously exposed to water-soluble CdSe/ZnS QDs and ICP-MS was used to measure the ^{111}Cd content to indicate the concentration of QDs in plasma, organs and excretion samples collected at predetermined time intervals [114].

Quantification of biomolecules by inductively coupled plasma mass spectrometry detection using nanoparticle labels

During the last few years new analytical tools based on the use of ICP-MS for the detection of biomolecules have been developed. However, despite the reported elemental advantages of ICP-MS, ICP-MS is not so sensitive for some elements of great importance in biomolecules (e.g. P and S) owing to their high ionisation potentials. Additionally, for such elements, isobaric overlaps from polyatomic ions of the same nominal m/z are common place. Thus, whereas metals can be readily detected at nanogram per litre levels, the detection limits for P and S are usually much worse. The use of high-resolution mass analysers or of ICP-MS instruments containing collision or reaction cells can overcome such problems to some degree [115].

Alternatively, the above-mentioned problems can be avoided if the biomolecule scrutinised is labelled with a metallic element or a metal NP containing elements easily detected by ICP-MS (e.g. a nanogold cluster), which is measured instead of P or S [116]. The idea behind such a strategy is to make biomolecules detectable by ICP-MS and thus benefit from its high sensitivity, isotopic ability, linearity and matrix robustness. This would allow the detection and determination of nearly all biomolecules, provided that the stoichiometry of the label and the efficiency of the bioconjugation reaction are known. Such an approach has been used to develop different ICP-MS-linked immunoassays which employ metal-NP-labelled antibodies as secondary antibodies in surface-linked immunoreactions.

Within the field of atomic spectrometry, the concept of elemental labelling with elemental nanostructures was pioneered some years ago by Zhang et al. [117] and by Baranov et al. [116]. However, this area of research is still of great novelty, with a high potential for future applications and continual development. In pioneer work, Zhang et al. [117] successfully demonstrated the determination of rabbit-anti-human immunoglobulin G (IgG) by ICP-MS using antibodies labelled with colloidal Au NPs. In this work, a sandwich-type immunoreaction was investigated as

the format for the measurement of the IgG. The antibody was first captured by immobilised human IgG, and then incubated with Au-NP-labelled goat-anti-rabbit IgG. Determination of Au was carried out by ICP-MS after elution with 2% HNO_3. In the same year, Baranov et al. [116] developed a set of novel immunoassays for the determination of different proteins using antibodies covalently labelled with 1.4-nm nanogold clusters. The immunoassays were directly coupled with ICP-MS detection to quantify the metal (Au) of the labelled antibodies. Four different immunoassay formats (using centrifugal filtration, protein A affinity, size-exclusion gel filtration or ELISA) coupled to the ICP-MS system were investigated, resulting in a high sensitivity and precision in the determinations of the proteins even in complex biological samples.

In a further development, Quinn et al. [118] successfully used element-labelled antibodies for the detection of two different proteins in a complex mixture. Labelling of two antibodies with Au NPs and a Eu cluster, respectively, allowed the simultaneous determination of two antigens with ICP-MS in a maleic anhydride plate immunoreaction, after appropriate digestion with 10% HCl. The reported results agreed well with those obtained using a conventional western blot, but a significantly higher precision was achieved with the ICP-MS approach for the determination in cultured cell lysates.

Merkoci et al. [119] proposed the use of ICP-MS for the sensitive detection of Au NPs used as labels for the determination of DNA in water samples. In this approach, Au NPs modified with anti-mouse IgG were used to trace oligonucleotides carrying a c-myc peptide. Oligonucleotide-peptide conjugates were first immobilised by UV radiation into a nitrocellulose membrane, then incubated with an anti-c-myc monoclonal antibody, followed by incubation with the secondary antibody (anti-mouse IgG) conjugated to Au NPs and, finally, the Au NP tracer was detected by ICP-MS after its appropriate dissolution with aqua regia (see the schematics of the proposed procedure in Fig. 6). The limit of detection for peptide-modified DNA was as low as 0.2 pmol for the oligonucleotide, a sensitivity approximately 40 times

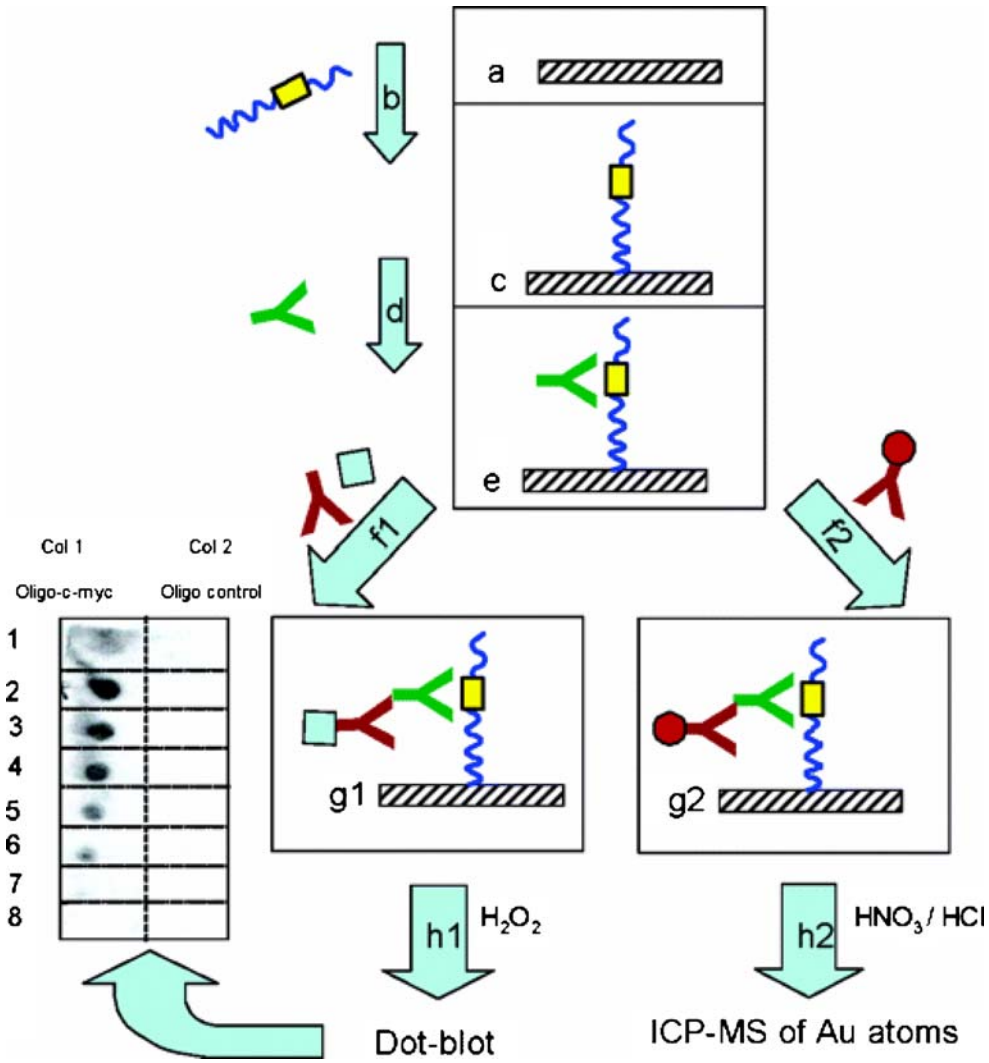

Fig. 6 The assay protocol. The nitrocellulose membrane (**a**) was introduced into the dot-blot manifold. The oligonucleotide carrying c-myc peptide (**b**) is immobilised over the membrane (**c**). It reacts overnight with the anti-c-myc (**d**). The immobilised oligonucleotide (**e**) is then treated: *1* according to the dot-blot assay and *2* according to the inductively coupled plasma mass spectrometry (*ICP-MS*)-linked assay. (From [119]; reproduced with permission of the American Chemical Society)

better than that achieved by the conventional dot-blot reference method. Thus, ICP-MS-based approach may have a significant potential for non-radioactive DNA detection and for the simultaneous determination of various sequences by multiple labelling with different kinds of inorganic NPs.

Separation techniques coupled with inductively coupled plasma mass spectrometry

An important goal in modern nanotechnology is the production of NPs with well-characterised sizes [120] because NPs have different physical and chemical characteristics depending on their size and shape [121]. Moreover, size distribution should be monitored to clarify whether the free NPs, aggregated particles, solutes or a mixture of these is present in the samples.

Analyses by TEM or X-ray photoelectron spectroscopy can give important information in terms of size distribution and chemistry of the NPs [105]. Unfortunately, in these cases the samples are analysed under a vacuum, an environment which is quite different from the native hydrated state of NPs in a colloidal dispersion. On the other hand, size characterisation studies of nanostructures using UV/vis or Raman spectroscopies might be significantly affected by the presence of unreacted species [122]. Isolation of the nanomaterials in their native dispersed state is therefore an important step in improving characterisation of NPs. Techniques for size distribution analysis of NPs in polydispersed samples include different separation techniques, such as flow-field fractionation (FFF) and size-exclusion chromatography (SEC) coupled with different spectroscopic detection techniques, including UV/vis spectroscopy, light scattering and ICP-MS.

Field-flow fractionation coupled with inductively coupled plasma mass spectrometry

FFF is a flow-assisted technique suited to separate colloidal nanosized particles by their hydrodynamic diameter [123, 124]. NPs can be fractionated with this separation technique according to their size. In this way, further characterisation of size-resolved NP fractions is possible. FFF techniques have been used to monitor the synthesis and growth of different NPs (such as water-soluble Au NPs or TiO_2 NPs) [125, 126] with different detectors. Characterisation of NPs by the on-line coupling of FFF with ICP-MS has also been described, allowing the development of a rather flexible method to characterise the size, polydispersity, and metal concentrations as a function of diameter [127, 128].

For example, alumina- and silica-based chemical mechanical polishing slurries were analysed to demonstrate the feasibility of FFF-ICP-MS to characterise NPs [127]. After FFF separation, ^{27}Al and ^{29}Si were measured by ICP-MS to obtain characteristic parameters such as size distributions, mean particle size, number-average, mass-average and *Z*-average diameters, minimum and maximum particle sizes, dominant particle size and particle size ranges. The mean particle sizes of alumina slurries varied between 150 and 350 nm. Silica slurries exhibited mean particle sizes ranging from 110 to 220 nm. ICP-MS measurements allowed the detection of the trace metals which were coeluted with Al and Si (or in the colloidal fractions) as well.

Bouby et al. [128] developed a method for the quantification of ICP-MS fractograms based on element mass flow. The quantification method was applied to the characterisation of synthetic CdSe/ZnS-mercaptoacetic acid core/shell-coated nanocrystals. Detection of Cd and Zn, the main elements used in the NP cores and shells, was performed by direct analysis with ICP-MS. The results obtained turned out to be useful for the determination of the geometric size of the NPs.

Chromatographic techniques coupled with inductively coupled plasma mass spectrometry

Among the separation techniques available for size distribution analysis of NPs present in polydispersed samples, FFF may yield good resolutions. It offers the possibility to separate colloidal matter ranging from 1 nm up to 100 μm and the fractionation process does not affect sample properties. However, it could be complex and time-consuming. On the other hand, liquid chromatography (e.g. SEC) can yield quantitative information about shape and nanocrystal size distributions (with separation resolutions less than 1 nm). Such information provided by SEC, added to its low cost, fast operation and reliability, make this

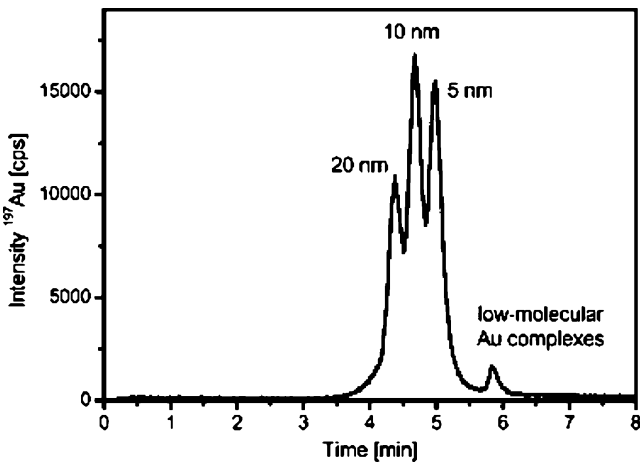

Fig. 7 High performance liquid chromatography chromatograms of Au nanoparticle standards. (From [130]; reproduced with permission of the Royal Society of Chemistry)

separation strategy an attractive option for standardising nanomaterials directly in the solution state [129].

As described already, Baranov et al. [116, 118] applied ICP-MS in combination with SEC to determine specific proteins via element-labelled antibodies and outlined the advantages of ICP-MS detection for Au NP detection. More recently, Helfrich et al. [130] proposed size characterisation of Au NPs by on-line coupling of liquid chromatography, or alternatively gel electrophoresis, with ICP-MS, as shown in Fig. 7. Gold colloids of 5–20-nm diameter were well separated on a standard C18 column owing to the size-dependent retention behaviour. With the retention time increasing proportionally to decreasing NP size on a logarithmic scale, unknown samples could be examined for their mean particle size by comparing them with colloidal standard solutions with well-defined size distributions. Gel electrophoresis was applied in a quite similar way, and in this case increased particle size resulted in increased migration times. The results were in good agreement with those obtained by complementary methods such as dynamic light scattering and TEM.

Coupling of liquid chromatography and ICP-MS for NP analysis has been proposed in innovative bioanalytical applications. Very recently, an analytical approach for DNA determination was proposed that is based on the labelling of biotinylated oligonucleotides with Au NPs bioconjugated with streptavidin. After a subsequent separation of the labelled conjugates by high-performance liquid chromatography, ICP-MS was used to detect the labels [131]. For accurate quantitative analysis of the Au-labelled oligonucleotides, it is essential to know how many Au atoms are bound and where. To satisfy those criteria, site-specific labelling is required and this was achieved by employing DNA biotinylated at the 59 end. The attached Au NPs were 1.4 nm in diameter and contained approximately 80 Au atoms covalently attached to a streptavidin protein and Alexa Fluor 488 fluorophore. In this way, the biomolecule signal was greatly enhanced owing to the higher sensitivity of ^{197}Au detection as compared with conventional ^{31}P detection. Interestingly, ICP-MS measurements can be utilised to establish mass balance for the NP label, thereby ensuring that all the labelled species from the bioconjugation reaction are detected and quantified.

Conclusions

Examples from various technological and science areas (including life sciences) in this review show that widespread inorganic MS techniques for direct solid analysis (e.g. LA-ICP-MS, GD-MS, SIMS and SNMS) may offer complementary spatial information (lateral and in-depth resolution) at the nanometre-length scale. The multielemental capabilities, isotopic information and high sensitivity common to all the inorganic MS techniques described above, as well as the rather easy quantification procedures using some of them, offer exceptional advantages for analytical characterisation at the nanoscale.

On the other hand, this review highlights the great potential of the ICP-MS system in the field of elemental characterisation of NPs, directly or after coupling to an appropriate separation system. In this sense, it is expected that the use of ICP-MS-based techniques providing accurate and precise measurements, informing on the size, elemental content of the NPs, isotopic ratios and evolution in time (all along the NP synthesis process), will start to grow in the near future, complementing other established characterisation tools.

In addition, the use of ICP-MS as a detector in bioassays offers significant benefits over more common and traditional methods. Low detection limits are expected with ICP-MS for biomolecules labelled with NPs (owing to the extremely high sensitivity of this detector and to the possibility of labelling a single biomolecule with several atoms constituting the NP). Moreover, by labelling different antibodies with different NPs, the simultaneous discrimination and determination of different biomolecules in a single sample becomes a reality.

One of the most promising applications of colloidal NPs in bioscience is bioconjugation of NPs with the desired biomolecules for "visualisation" of such molecules in biological tissues and cells. Unfortunately the state of the art of such analytical development is still far from being quantitative. The analytical potential of NPs as labels for quantitative analysis of biomolecules relies on eventual knowledge/determination of the NP–biomolecule stoichiometry and here again ICP-MS could play a pivotal role. Much more research in this direction and in the use of ICP-MS in future biotoxicology studies can be envisaged.

Acknowledgements Financial support from "Plan Nacional de I+D+I" (Spanish Ministry of Science and Innovation, and FEDER Programme) through the projects CTQ2006-02309/BQU and MAT2007-65097-C02-01 is gratefully acknowledged. In addition, B.F. acknowledges financial support from the "Juan de la Cierva" Research Programme of the Ministry of Science and Innovation of Spain. Both programmes are cofinanced by the European Social Fund.

References

1. Norris JL, Cornett DS, Mobley JA, Andersson M, Seeley EH, Chaurand P, Caprioli RM (2007) Int J Mass Spectrom 260:212–221
2. Mas S, Perez R, Martinez-Pinna R, Egido J, Vivanco F (2008) Proteomics 8:3735–3745
3. Becker JS, Zoriy M, Wu B, Matusch A, Becker JS (2008) J Anal At Spectrom 23:1275–1280
4. Pisonero J, Günther D (2008) Mass Spectrom Rev 27:609–623

5. Hoffmann V, Kasik M, Robinson PK, Venzago C (2005) Anal Bioanal Chem 381:173–188
6. Nygren H, Malmberg P (2007) Trends Biotechnol 25:499–504
7. Touboul D, Halgand F, Brunelle A, Kersting R, Tallarek E, Hagenhoff B, Laprevote O (2004) Anal Chem 76:1550–1559
8. Becker JS, Matusch A, Depboylu C, Dobrowolska J, Zoriy MV (2007) Anal Chem 79:6074–6080
9. Becker JS, Zoriy M, Becker JS, Dobrowolska J, Matusch A (2007) J Anal At Spectrom 22:736–744
10. Hwang DJ, Grigoropoulos CP, Yoo J, Russo RE (2006) Appl Phys Lett 89:254101
11. Bubert H, Jenett H (2002) Surface and thin film analysis. Wiley-VCH, Weinheim
12. Barshik CM, Duckworth DC, Smith DH (2000) Inorganic mass spectrometry. Wiley, New York
13. Becker JS (2008) Inorganic mass spectrometry: principles and applications. Wiley, New York
14. Betti M (2005) Int J Mass Spectrom 242:169–182
15. Fernández B, Claverie F, Pecheyran C, Donard OFX (2007) Trends Anal Chem 26:951–966
16. Gray AL (1985) Analyst 110:551–556
17. Horlick G, Montaser A (1998) In: Montaser A (ed) Inductively coupled plasma mass spectrometry. Wiley-VCH, New York, pp 543–547
18. Becker JS (2002) Spectrochim Acta Part B 57:1805–1820
19. Durrant SF (1999) J Anal At Spectrom 14:1385–1403
20. Hattendorf B, Latkoczy C, Günther D (2003) Anal Chem 75:341A–347A
21. Günther D, Hattendorf B (2005) Trends Anal Chem 24:255–265
22. Guillong M, Günther D (2002) J Anal At Spectrom 17:831–837
23. Koch J, Günther D (2007) Anal Bioanal Chem 387:149–153
24. Kroslakova I, Günther D (2007) J Anal At Spectrom 22:51–62
25. Garcia CC, Lindner H, von Bohlen A, Vadla C, Niemax K (2008) J Anal At Spectrom 23:470–478
26. Garcia CC, Lindner H, Niemax K (2009) J Anal At Spectrom 24:14–26
27. Hergenröder R, Samek O, Hommes V (2006) Mass Spectrom Rev 25:551–572
28. Margetic V, Bolshov M, Stockhaus A, Niemax K, Hergenröder R (2001) J Anal At Spectrom 16:616–621
29. Margetic V, Niemax K, Hergenröder R (2003) Anal Chem 75:3435–3439
30. Pisonero J, Koch J, Wälle M, Hartung W, Spencer ND, Günther D (2007) Anal Chem 79:2325–2333
31. Mateo MP, Garcia CC, Hergenröder R (2007) Anal Chem 79:4908–4914
32. Stöckle R, Setz P, Deckert V, Lippert T, Wokaun A, Zenobi R (2001) Anal Chem 73:1399–1402
33. Wen S-B, Greif R, Russo RE (2007) Appl Phys Lett 91:251113
34. Hwang DJ, Jeon H, Grigoropoulos CP, Yoo J, Russo RE (2008) J Appl Phys 104:013110
35. Becker JS, Gorbunoff A, Zoriy M, Izmer A, Kayser M (2006) J Anal At Spectrom 21:19–25
36. Zoriy M, Kayser M, Becker J (2008) Int J Mass Spectrom 273:151–155
37. Borisova AY, Freydier R, Polvé M, Salvi S, Candaudap F, Aigouy T (2008) Geostand Geoanal Res 32:209–229
38. Halter WE, Pettke T, Heinrich CA (2004) Contrib Mineral Petrol 147:385–396
39. Horvath M, Guillong M, Izmer A, Kivel N, Restani R, Günther-Leopold I, Opitz Coutureau J, Hellwig C, Günther D (2007) J Anal At Spectrom 22:1266–1274
40. Becker JS, Sela H, Dobrowolska J, Zoriy M, Becker JS (2008) Int J Mass Spectrom 270:1–7
41. Gligorovski S, Van Elteren JT, Grgic I (2008) Sci Total Environ 407:594–602
42. Wu B, Zoriy M, Chen Y, Becker JS (2009) Talanta 78:132–137
43. Dobrowolska J, Dehnhardt M, Matusch A, Zoriy M, Palomero-Gallagher N, Koscielniak P, Zilles K, Becker JS (2008) Talanta 74:717–723
44. Becker JS, Dietrich RC, Matusch A, Pozebon D, Dressler VL (2008) Spectrochim Acta Part B 63:1248–1252
45. Wu B, Chen Y, Becker JS (2009) Anal Chim Acta 633:165–172
46. Pisonero J, Fernández B, Pereiro R, Bordel N, Sanz-Medel A (2006) Trends Anal Chem 25:11–18
47. Winchester R, Payling R (2004) Spectrochim Acta Part B 59:607–666
48. Nelis T, Aeberhard M, Hohl M, Rohr L, Michler J (2006) J Anal At Spectrom 21:112–125
49. Martín A, Pereiro R, Bordel N, Sanz-Medel A (2007) J Anal At Spectrom 22:1179–1183
50. Steiner RE, Lewis CL, King F (1997) Anal Chem 69:1715–1721
51. Yang C, Ingenieri K, Mohill M, Harrison WW (2000) J Anal At Spectrom 15:73–78
52. Gendt S, Van Greiken RE, Ohorodnik SK, Harrison WW (1996) Anal Chem 67:1026–1033
53. Vazquez M, Pisonero J, Costa JM, Pereiro R, Bordel N, Sanz-Medel A (2003) J Anal At Spectrom 18:612–617
54. Pisonero J (2006) Anal Bioanal Chem 384:47–49
55. Nelis T (2006) Appl Spectros Rev 41:227–258
56. Hoffmann V, Dorka R, Wilken L, Hodoroaba V, Wetzig K (2003) Surf Interface Anal 35:575–582
57. Shimizu K, Payling R, Habazaki H, Skeldon P, Thompson GE (2004) J Anal At Spectrom 19:692–695
58. Lewis CL, Moser MA, Dale DE, Hang W, Hassell C, King FL, Majidi V (2003) Anal Chem 75:1983–1996
59. Fliegel D, Waddell R, Majidi V, Günther D, Lewis CL (2005) Anal Chem 77:1847–1852
60. Muñiz AC, Pisonero J, Lobo L, Gonzalez C, Bordel N, Pereiro R, Tempez A, Chapon P, Tuccitto N, Licciardello A, Sanz-Medel A (2008) J Anal At Spectrom 23:1239–1246
61. Hohl M, Kanzari A, Michler J, Nelis T, Fuhrer K, Gonin M (2006) Surf Interface Anal 38:292–295
62. Tuccitto N, Lobo L, Tempez A, Delfanti I, Chapon P, Canulescu S, Bordel N, Michler J, Licciardello A (2009) Rapid Commun Mass Spectrom 23:549–556
63. Canulescu S, Whitby J, Fuhrer K, Hohl M, Gonin M, Horvart T, Michler J (2009) J Anal At Spectrom 24:178–180
64. Lewis C, Doorn SK, Wayne DM, King FL (2000) Appl Spectrosc 54:1236–1244
65. Naeem TM, Matsuta H, Wagatsuma K (2004) Anal Sci 20:1717–1720
66. Tarik M, Lotito G, Whitby JA, Koch J, Fuhrer K, Gonin M, Michler J, Bolli JL, Günther D (2009) Spectrochim Acta Part B 64:262–270
67. Shelley JT, Ray SJ, Hieftje GM (2008) Anal Chem 80:8308–8313
68. Benninghoven A, Rüdenauer FG, Werner HW (1987) Secondary ion mass spectrometry: basic concepts, instrumental aspects, applications and trends. Wiley, New York
69. Vickerman JC (1998) Surface analysis—the principal techniques. Wiley, Chichester
70. Walker AV (2008) Anal Chem 80:8865–8870
71. Nygren H, Malmberg P, Kriegeskotte C, Arlinghaus HF (2004) FEBS Lett 566:291–293
72. Benninghoven A (1994) Angew Chem 33:1023–1043
73. Aoyagi S (2009) Surf Interface Anal 41:136–142
74. Anderson O, Sheumann V, Rothlaar U, Rupertus V (2004) Glass Sci Technol 77:159–165

75. Jones EA, Lockyer NP, Vickerman JC (2008) Anal Chem 80:2125–2132
76. Arlinghaus HF, Kriegeskotte C, Fartmann M, Wittig A, Sauerwein W, Lipinsky D (2006) Appl Surf Sci 252:6941–6948
77. Chandra S (2008) Appl Surf Sci 255:1273–1284
78. Heeren RMA, Kükrer-Kaletas B, Taban IM, MacAleese L, McDonnell (2008) Appl Surf Sci 255:1289–1297
79. Graf N, Gross T, Wirth T, Weigel W, Unger WES (2009) Anal Bioanal Chem 393:1907–1912
80. Barnes JP, Carreau V, Maitrejean S (2008) Appl Surf Sci 255:1564–1568
81. Nojima M, Toi M, Maekawa A, Tomiyasu B, Sakamoto T, Owari M, Nihei Y (2004) Appl Surf Sci 231:930–935
82. Guerquin-Kern JL, Wu TD, Quintana C, Croisy A (2005) Biochim Biophys Acta 1724:228–238
83. Besmehn A, Hoppe P (2003) Geochim Cosmochim Acta 67:4693–4703
84. Audinot JN, Schneider S, Yegles M, Hallegot P, Wenning R, Migeon HN (2004) Appl Surf Sci 231:490–496
85. Quintana C, Bellefqih S, Laval JY, Guerquin-Kern JL, Wu TD, Avila J, Ferrer I, Arranz R, Patiño C (2006) J Struct Biol 153:42–54
86. Nakata Y, Honda Y, Ninomiya S, Seki T, Auki T, Matsuo J (2009) J Mass Spectrom 44:128–136
87. Mikuba R, Hassaballa S, Uchino K, Yurimoto H, Todokoro R, Kumondai K, Ishihara M (2008) Appl Surf Sci 255:1595–1598
88. Fartmann M, Dambach S, Kriegeskotte C, Lipinsky D, Wiesmann HP, Wittig A, Sauerwein W, Arlinghaus HF (2003) Appl Surf Sci 203:726–729
89. Fartmann M, Kriegeskotte C, Dambach S, Wittig A, Sauerwein W, Arlinghaus HF (2004) Appl Surf Sci 231:428–431
90. Arlinghaus HF, Fartmann M, Kriegeskotte C, Dambach S, Wittig A, Sauerwein W, Lipinsky D (2004) Surf Interface Anal 36:698–701
91. Kriegeskotte C, Möller J, Lipinsky D, Wittig A, Sauerwein W, Haier J, Arlinghaus HF (2006) Surf Interface Anal 38:121–125
92. Wittig A, Arlinghaus HF, Kriegeskotte C, Moss RL, Appelman K, Schmid KW, Sauerwein WAG (2008) Mol Cancer Ther 7:1763–1771
93. Konarski P, Kaczorek K, Cwil M, Marks J (2008) Vacuum 82:1133–1136
94. Kirchner U, Vogt R, Natzeck C, Goschnick J (2003) Aerosol Sci 34:1323–1346
95. Pinnick V, Rajagopalachary S, Verkhoturov SV, Kaledin L, Schweikert EA (2008) Anal Chem 80:9052–9057
96. Goschnick J, Natzeck C, Sommer M, Zudock F (1998) Thin Solid Films 332:215–219
97. Hodoroaba V, Unger WES, Jenett H, Hoffmann V, Hagenhoff B, Kayser S, Wetzig K (2001) Appl Surf Sci 179:30–37
98. Kothleitner G, Rogers M, Berendes A, Bock W, Kolbesen BO (2005) Appl Surf Sci 252:66–76
99. Schneider T, Sommer M, Goschnick J (2005) Appl Surf Sci 252:257–260
100. Katona GL, Berenyi Z, Peter L, Vad K (2008) Vacuum 82:270–273
101. Escobar R, Gago R, Lousa A, Albella JM (2009) Trends Anal Chem 28:494–505
102. Thomas R (2002) Spectroscopy 17:26–33
103. Ammann AA (2007) J Mass Spectrom 42:419–427
104. Sanz-Medel A, Montes-Bayon M, Fernandez de la Campa MR, Ruiz-Encinar J, Bettmer J (2008) Anal Bioanal Chem 390:3–16
105. Peng X, Schlamp MC, Kadavanich AV, Alivisatos AP (1997) J Am Chem Soc 119:7019–7029
106. Bang JH, Suh WH, Suslik KS (2008) Chem Mater 20:4033–4038
107. Degueldre C, Favarger PY, Wold S (2006) Anal Chim Acta 555:263–268
108. Moreels I, Lambert K, De Muynck D, Vanhaecke F, Poelman D, Martins JC, Allan G, Hens Z (2007) Chem Mater 19:6101–6106
109. Montoro Bustos AR, Ruiz Encinar J, Fernández-Argüelles MT, Costa JM, Sanz-Medel A (2009) Chem Commun . doi:10.1039/b901493d
110. Calero-DdelC VL, Rinaldi C (2007) J Magn Magn Mater 314:60–67
111. Sonavanea G, Tomoda K, Makinoa K (2008) Colloids Surf B Biointerfaces 66:274–280
112. De Jong WH, Hagens WI, Krystek P, Burger MC, Sips AJAM, Geertsma RE (2008) Biomaterials 29:1912–1919
113. Tang J, Xiong L, Wang S, Wang J, Liu L, Li J, Wanc Z, Xi T (2008) Appl Surf Sci 255:502–504
114. Chen Z, Chen H, Meng H, Xing G, Gao X, Sun B, Shi X, Yuan H, Zhang C, Liu R, Zhao F, Zhao Y, Fang X (2008) Toxicol Appl Pharmacol 230:364–371
115. Tanner SD, Baranov VI, Bandura DR (2002) Spectrochim Acta Part B 57:1361–1452
116. Baranov VI, Quinn ZA, Bandura DR, Tanner SD (2002) Anal Chem 74:1629–1636
117. Zhang C, Zhang ZY, Yu BB, Shi JJ, Zhang XR (2002) Anal Chem 74:96–99
118. Quinn ZA, Baranov VI, Tanner SD, Wrana JL (2002) J Anal At Spectrom 17:892–896
119. Merkoci A, Aldavert M, Tarrason G, Eritja R, Alegret S (2005) Anal Chem 77:6500–6503
120. Schmid G (2003) Nanoparticles: from theory to application. Wiley-VCH, Weinheim
121. Alivisatos AP (1996) Science 271:933–937
122. Aryal S, Remant BKC, Dharmaraj N, Bhattarai N, Kim CH, Kim HY (2006) Spectrochim Acta Part A 63:160
123. Roda B, Zattoni A, Reschiglian P, Moon MH, Mirasoli M, Michelini E, Roda A (2009) Anal Chim Acta 635:132–143
124. Reschiglian P, Zattoni A, Roda B, Michelini E, Roda A (2005) Trends Biotechnol 23:475–483
125. Rameshwar T, Samal S, Lee S, Kim S, Cho J, Kim IS (2006) J Nanosci Nanotechnol 6:2461–2467
126. Contado C, Pagnoni A (2008) Anal Chem 80:7594–7608
127. Siripinyanond A, Barnes RM (2002) Spectrochim Acta Part B 57:1885–1896
128. Bouby M, Geckeis H, Geyer FW (2008) Anal Bioanal Chem 392:1447–1457
129. Krueger KM, Al-Somali AM, Falkner JC, Colvin VL (2005) Anal Chem 77:3511–3515
130. Helfrich A, Bruchert W, Bettmer J (2006) J Anal At Spectrom 21:431–434
131. Kerr SL, Sharp B (2007) Chem Commun 4537–4539